CONF-75-102-E
E-0031

Expt. #31A

ANL-HEP-CP-75-39

Submitted to the 1975 International Symposium on Lepton and Photon Interactions, August 21-27, Stanford University
Subject Heading: Experimental Neutrino Physics

Antineutrino-Proton Interactions in the 15-Foot Bubble Chamber*

S. J. BARISH, M. DERRICK, T. DOMBECK, L. HYMAN, K. JAEGER, D. LISSAUER, R. MILLER, B. MUSGRAVE, J. PHELAN, P. SCHREINER and R. SINGER

Argonne National Laboratory, Argonne, Illinois 60439

and

A. ENGLER, G. KEYES, R. KRAEMER and J. SCHLERETH

Carnegie-Mellon University, Pittsburgh, Pennsylvania 15213

From 24,000 pictures of the Fermilab 15-foot hydrogen bubble chamber exposed to a broad band $\bar{\nu}$ beam, we have obtained 89 $\bar{\nu}p \rightarrow \mu^+ + X^0$ events with a total momentum in the charged tracks greater than 5 GeV/c. We discuss the techniques used to identify the muon and estimate the $\bar{\nu}$ energy. The charged particle multiplicity distributions and the mean π^0 multiplicity are presented. The semi-inclusive X, Y, Z, Q^2 and W distributions are compared with model predictions. The rate of strange particle production is measured. We find no evidence for charm particle production.

---

*Work supported by the U. S. Energy Research and Development Administration.

We present preliminary results on antineutrino-proton interactions as observed in the Fermilab 15-foot bubble chamber filled with hydrogen. These data were obtained from an analysis of 24,000 pictures. The antineutrino/neutrino beam was formed from a 300 GeV extracted proton beam, which was focused onto a 30 cm long $A\ell$ target. The produced negative (positive) particles were focused (defocused) by a single-stage pulsed magnetic "horn" operating at a current of 140 kA. The resulting $\bar{\nu}$ and ν fluxes at the 15-foot chamber are calculated to be as shown in Fig. 1. The $\bar{\nu}$ energy spectrum peaks at $\sim$ 14 GeV and the $\bar{\nu}/\nu$ flux ratio crosses through unity near 75 GeV. The average proton intensity for our run was 0.7×10^{13} protons/pulse. We estimate the uncertainty in the flux at this time to be about a factor of two.

The first scan of the film was done mostly by physicists at a magnification of one-third life size. All events except for one-prongs which have a visible momentum in the forward hemisphere of greater than 2 GeV/c were recorded. Three-prongs (and only three-prongs) which had a track in the backward (anti-beam) 45° cone were not recorded in order to reduce the large background coming from charged hadron scatters. The scanning efficiency is $> 90\%$ except for the one-prong topology for which a separate scan of the film is under way. It should be noted that all physics distributions in this paper (except for Fig. 12) do not include one-prongs.

To reconstruct the tracks, a modified version of the ANL 12-foot

chamber TVGP was used. After repeated measurements, the event pass rate inside a 19 m^3 fiducial volume was 89%. All events were re-examined by a physicist after measurement. The kinematic fitting of the events was performed using the program SQUAW.

Events can be grouped into four classes:

(I) $\bar{\nu}p \rightarrow \mu^+ + \ldots$

(II) $\nu p \rightarrow \mu^- + \ldots$

(III) $\bar{\nu}p \rightarrow \bar{\nu} + \ldots, \quad \nu p \rightarrow \nu + \ldots$

(IV) $np \rightarrow NN + \ell\pi$.

In this paper, we report results on the events in Classes I and II - the charged-current antineutrino and neutrino interactions, but only from the three-prong and higher topologies. To minimize contamination from events of Classes III and IV, we impose an energy selection such that all events with total momentum in the charged tracks less than 5 GeV/c are rejected. The neutron-induced background for events of visible momentum greater than 5 GeV/c has been measured from fitted $np \rightarrow pp\pi^-$ events to be only a few percent. This can be seen in Fig. 2 which shows the momentum spectrum of the $np \rightarrow pp\pi^-$ events. The rapid decrease in the neutron intensity with increasing momentum is expected from results obtained at neutrino beams at ANL and CERN.

The identification of the muon track is, of course, crucial. For the bulk of our running (200, 000 approved pictures), we will use the External

Muon Detector developed by the Berkeley-Hawaii groups[1] to identify the muons. For the present analysis, we have used a muon selection method which was developed from a Monte Carlo study of the Class I, II, and III type events. Fig. 3 is a flow chart that shows the muon selection technique. From the Monte Carlo, we expect the selected sample of μ^+ tracks to include 96% of all μ^+ tracks, but that it will also contain about 12% contamination from events of Classes II and III. Secondary scattering of the selected muon track is a direct measure of the hadron contamination in the sample of Type I and II events. We find 1 μ^+ and 0 μ^- tracks which scatter in a sample of 89 μ^+ and 37 μ^- tracks. From the measured muon track length in the liquid and known $\pi^{\pm}$p interaction lengths, we determine the 90% CL upper limit for misidentified muons to be 9%.

An important problem in neutrino experiments using low Z material for a target is the determination of the beam energy for each event. We have considered two methods to estimate E_ν. First, we have used the Burmeister-Cundy-Myatt[2] technique of assuming the neutral hadrons follow the direction of the charged hadron system; thus, E_ν is just given by

$$E_\nu = P_L^\mu + P_\perp^\mu P_L^H / P_\perp^H \quad .$$

From Monte Carlo studies, we find the resolution to be about ±15%. The second method is to do "0C" calculations: We assume that there is one missing π^o or neutron in each event, and then use energy and momentum conservation to calculate E_ν, taking the average of the two values for those events

in which we do not identify a nucleon or all the pions in the final state. This second method tends to give values of E_ν that are not very much larger than P_{VIS}. The Burmeister-Cundy-Myatt method, however, can give very large and erroneous values of E_ν when $P_\perp^H$ is small. Fig. 4a compares E_ν^{BCM} with E_ν^{0C} for a sample of μ^+ events. Although the differences can often be quite large, there is a good correlation between the results of the two methods on the average.

One can also study the errors on the E_ν estimation by deleting the charged tracks from high multiplicity events and treating them as lower multiplicity events. We have changed five-prong events into three-prong events and seven-prong events into five-prong events. Figs. 4b and c show the visible energy for the actual events compared with the neutrino energy determined by the 0C method for the "track-deleted" events. The correlation is good. We have also studied the 0C method in our lower energy Argonne neutrino experiment[3] and find that it gives a good estimate of E_ν in most cases. We therefore use this 0C technique for estimating E_ν in this paper. Fig. 5 displays the energy distributions of our μ^+ and μ^- type events.

Fig. 6 shows the charged particle multiplicity distributions for μ^+ events; the cross-hatched events have $E_{\bar{\nu}} > 30$ GeV. We find that for $E_{\bar{\nu}} > 5$ GeV, $\langle n_C^H \rangle_{\mu^+} = 3.17 \pm 0.17$, with the one-prong topology excluded. From our partial one-prong scan and the shape of the Y distribution (shown below), we expect an upper limit of 27 one-prong events in our film; this results in

a lower limit on $\langle n_C^H \rangle$ of 2.66 ± 0.16.

Fig. 7a shows the distribution of invariant mass W recoiling from the positive muon tracks. No significant fine structure is apparent. The cross-hatched events have Q^2 - the four-momentum transfer between the leptons - less than 2 $(GeV/c)^2$; they occur at low W values as one would expect for N^* production.

Fig. 8a displays the Q^2 distribution for all μ^+ events. The shaded events have W less than 3 GeV and they clearly dominate the low Q^2 region.

Fig. 7b shows the multiplicity as a function of W; the correlation is strong and of a positive sign.

Fig. 8b shows the charged-particle multiplicity as a function of Q^2; here the dependence is quite weak. In these distributions, it should be noted that the missing one-prong events are expected to contribute at small Q^2 and W values.

In order to examine the predictions of the parton model, we have considered four more distributions. Fig. 9 shows the average value of Q^2 as a function of E_ν; the predicted linear rise with $E_{\bar{\nu}}$ is observed, with a slope of 0.16 ± 0.02.

Fig. 10a shows the $Y = 1 - E_\mu / E_\nu$ distribution for antineutrino events; events with $E_{\bar{\nu}} > 30$ GeV are shown cross-hatched. The curve represents the expected $(1 - Y)^2$ shape. We believe that the dip at small Y is due to the

fact that we have not included the one-prong events, which are expected to contribute mainly at low Y. Figs. 10b, c, d show the Y distribution as a function of multiplicity; lower n_{CH} events are clearly correlated with low Y values. For comparison, Fig. 10e shows the neutrino (μ^-) Y distribution; it is consistent with being flat although some μ's at large Y are no doubt being lost because of the muon selection methods. It should be remembered that the Y measurement is sensitive to the beam energy determination.

Fig. 11 shows the $X' = Q^2/(2M\nu + M^2)$ distribution compared with SLAC electroproduction data.[4] The agreement is fair.

As a further test of the parton model, we have plotted in Fig. 12 the average π^- multiplicity in our μ^+ events as a function of $Z\,[Z = E_{\pi^-}/(E_{\bar{\nu}} - E_{\mu^+})]$. We have estimated the one-prong loss to be 20% in calculating σ_T. The curves are predictions by L. Sehgal[5] for $\bar{\nu}$ and ν nucleon interactions in the current fragmentation region ($Z > 0.2$). The predictions amount to a determination of the parton fragmentation functions from electroproduced pion data. The agreement between our $\bar{\nu}p$ data and the electroproduction data interpreted by the parton model is good, particularly since it is not just the shape but the absolute value that is predicted.

We have also measured the inclusive π^o, Λ^o, and K_s^o production rates. From a sample of 24 converted γ's, 7 $\Lambda^o \to p\pi^-$ decays, and 4 $K_s^o \to \pi^+\pi^-$ decays, we find the inclusive rates

$$\frac{\sigma(\mu^+\pi^o + \ldots)}{\sigma(\mu^+)} = 2.14 \pm 0.52$$

$$\frac{\sigma(\mu^+\Lambda^o + \ldots)}{\sigma(\mu^+)} = 0.14 \pm 0.06$$

$$\frac{\sigma(\mu^+K^o + \ldots)}{\sigma(\mu^+)} = 0.15 \pm 0.08 \quad .$$

The π^o value may be compared to the mean number of negative particles $\langle n_- \rangle = 1.58 \pm 0.09$. For 25 GeV/c $\pi^+ p$ interactions[6], $\sigma(\pi^+ p \to \Lambda + \ldots)/\sigma(\pi^+ p \to \text{all}) = 0.033 \pm 0.004$, which is much lower than our $\bar{\nu} p$ result. The cross-hatched events in Fig. 5a show the energy distribution of our detected strange particle events; none of these events gave a constrained kinematic fit at the production origin.

Finally, we have made a preliminary search for charm particles by measuring the invariant masses of all particle combinations and have found no significant structure at high mass. The large number of possible mass combinations prohibits us from displaying these distributions. In any case, it is clear that charm particle production is not dominating high energy $\bar{\nu} p$ interactions.

In summary, we have presented the first look at charged-current antineutrino-proton interactions in the 10-40 GeV energy region. Our preliminary data agree well with the predictions of the quark-parton model. The results suggest that the rate of strange particle production is larger than one

would have naively expected. No evidence for charm particle production is observed. These results represent only a few percent of the approved exposure and we eagerly anticipate a large increase in statistics, which will allow for more detailed physics conclusions.

References

1. F. Harris et al., Nucl. Inst. and Methods 103, 345 (1972).

2. G. Myatt, CERN/ECFA/72-4, Vol. II, p. 117.

3. S. Barish et al., "An Inclusive Look at νp and νn Charged Current Reactions Below 6 GeV," Argonne-Purdue Collaboration, paper submitted to this conference.

4. J. Poucher et al., Phys. Rev. Letters 32, 118 (1974).

5. L. Sehgal, Nucl. Physics B90, 471 (1975).

6. J. Waters et al., Nucl. Physics B17, 448 (1970).

Figure Captions

Fig. 1 The calculated $\bar{\nu}$ and ν fluxes.

Fig. 2 The neutron momentum distribution for fitted $np \rightarrow pp\pi^-$ events.

Fig. 3 Flow chart used for muon selection.

Fig. 4a Comparison of $E_{\bar{\nu}}$ as calculated by the Burmeister-Cundy-Myatt method and the "0C" method.

b, c Comparison of $E_{\bar{\nu}}$ for real events and track-deleted events.

Fig. 5 Energy distribution of μ^+ and μ^- events as calculated using 0C method. The cross-hatched μ^+ events have seen strange particles.

Fig. 6 The charged-particle multiplicity for μ^+ events; cross-hatched events have $E_{\bar{\nu}} > 30$ GeV.

Fig. 7 (a) The W distribution for $\bar{\nu}$ events; cross-hatched events have $Q^2 < 2\,(\mathrm{GeV}/c)^2$. (b) The charged-hadron multiplicity as a function of W; the one-prong topology is not included.

Fig. 8 (a) The Q^2 distribution for $\bar{\nu}$ events; cross-hatched events have $W < 3$ GeV. (b) The charged-hadron multiplicity as a function of Q^2; the one-prong topology is not included.

Fig. 9 Average value of Q^2 as a function of $E_{\bar{\nu}}$.

Fig. 10 The $Y = 1 - E_\mu/E_\nu$ distributions for antineutrino (a-d) and neutrino (e) events.

Fig. 11 The $X' = Q^2/(2M\nu + M^2)$ distribution for $\bar{\nu}$ events.

Fig. 12 The Z distribution for negative tracks (assumed to be π^-) for the $\bar{\nu}$ events. Curves are from Ref. 5.

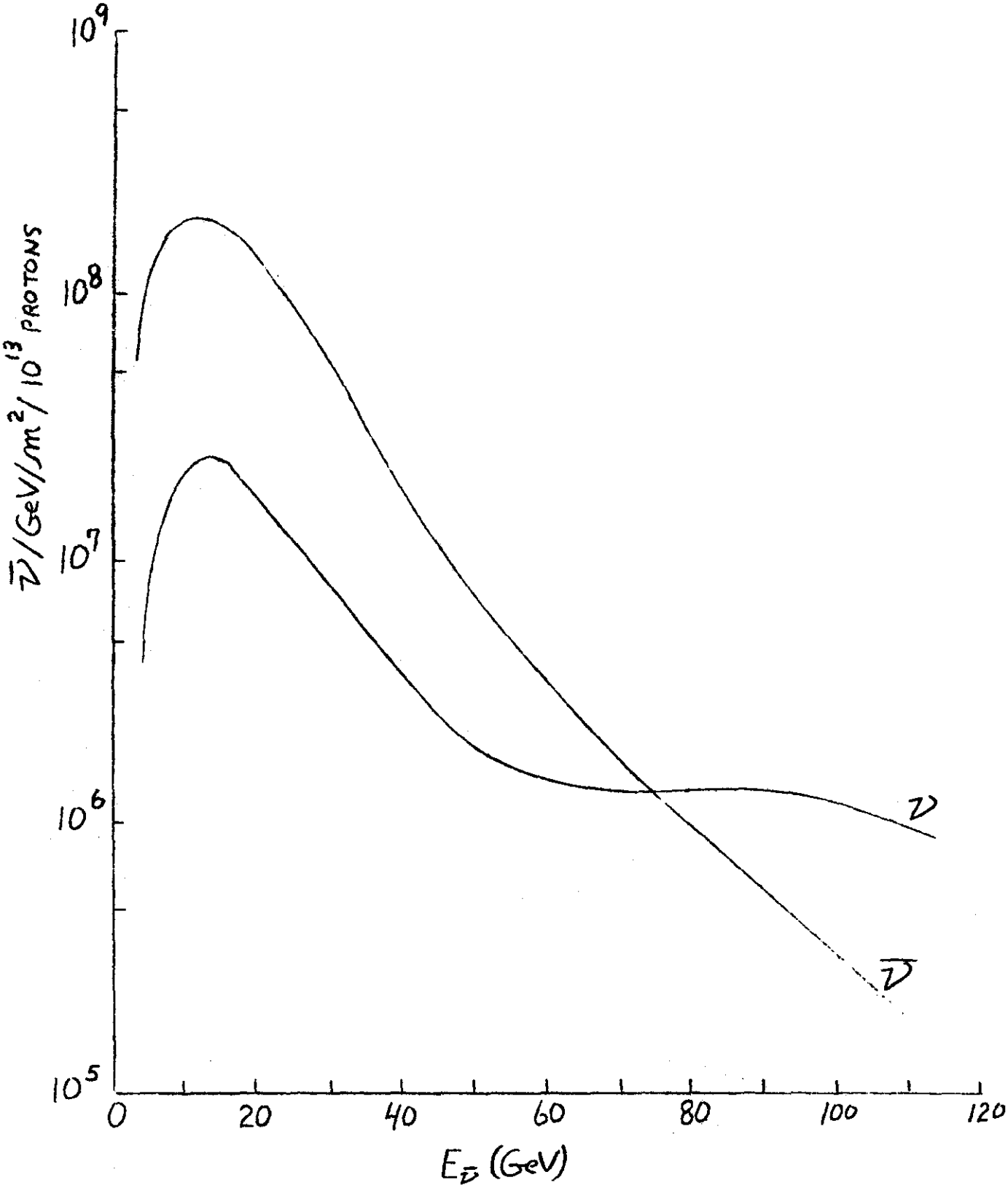
10^9
10^8
10^7
10^6
10^5
$\bar{\nu}$/GeV/m^2/10^{13} PROTONS
0
20
40
60
80
100
120
$E_{\bar{\nu}}$ (GeV)
ν
$\bar{\nu}$

Fig. 1

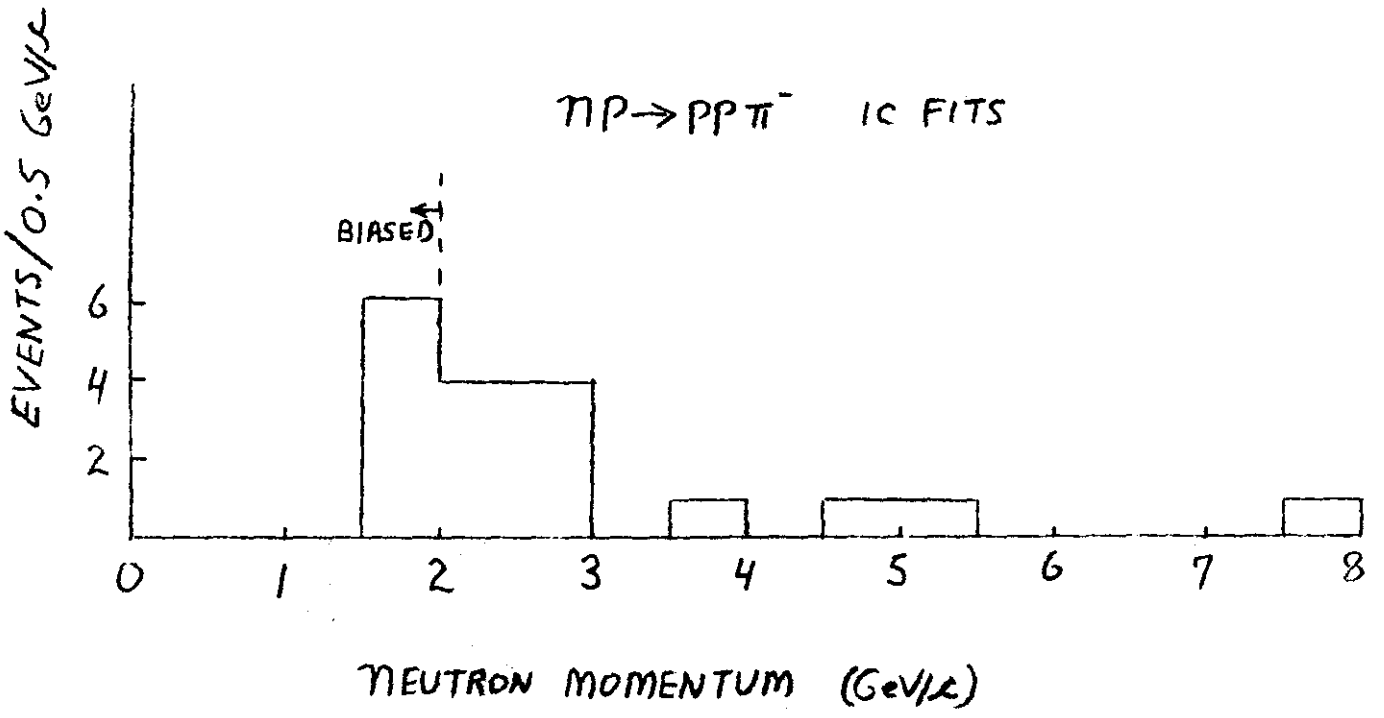
$np \to pp\pi^-$ 1C FITS
BIASED
EVENTS/0.5 GeV/c
2
4
6
0
1
2
3
4
5
6
7
8
NEUTRON MOMENTUM (GeV/c)

Fig. 2

Definitions :

$$R = \frac{\text{Largest Momentum Track}}{\text{Second Largest Mom. Track}}$$

$P_{\perp}^{M}$ = Largest Transverse Momentum Relative to $\bar{\nu}$ Direction

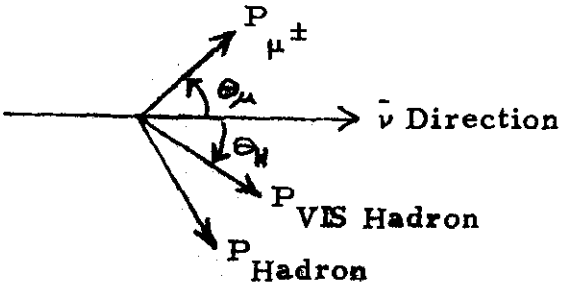

Modified Burmeister-Cundy Method

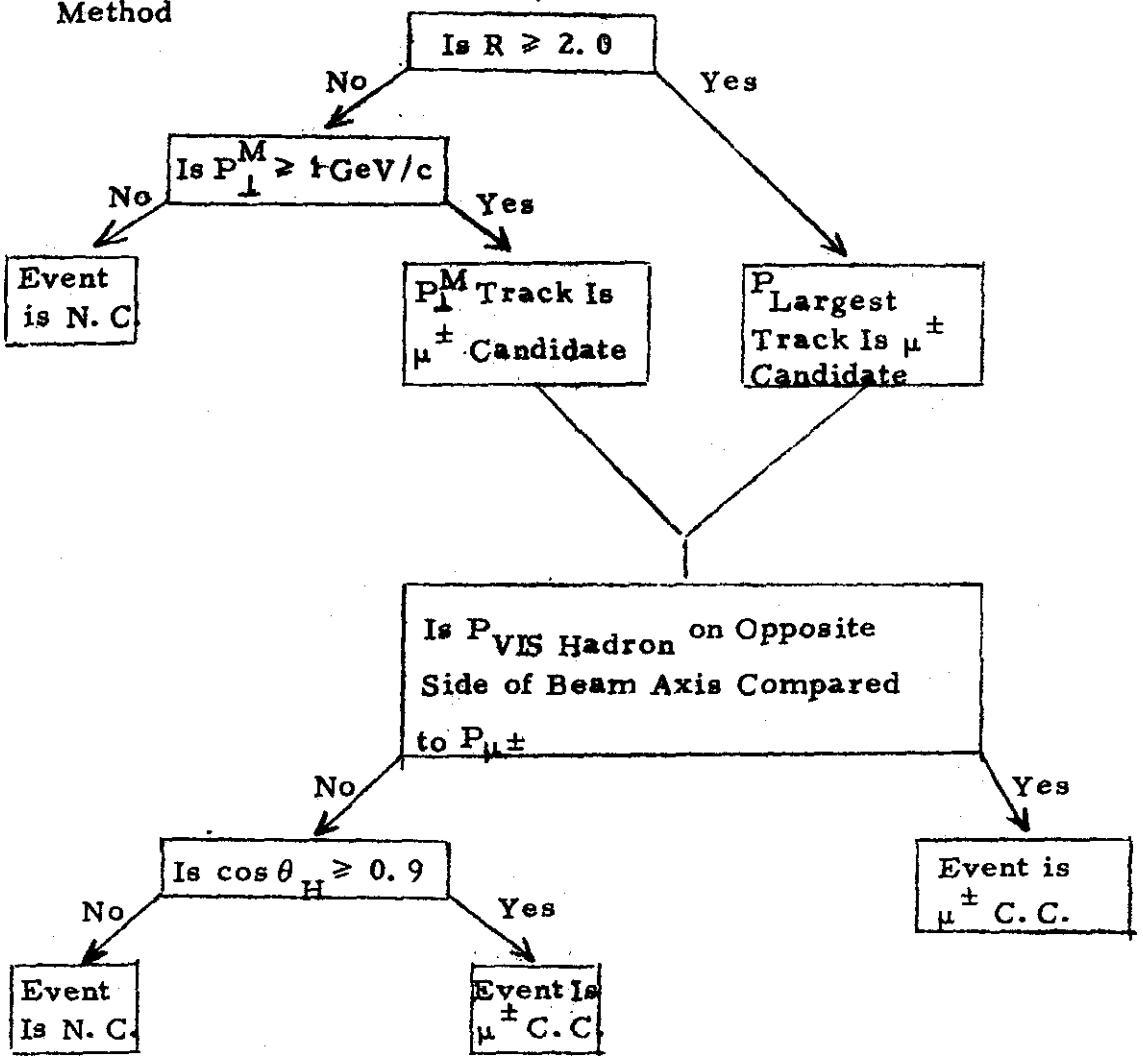

Fig. 3

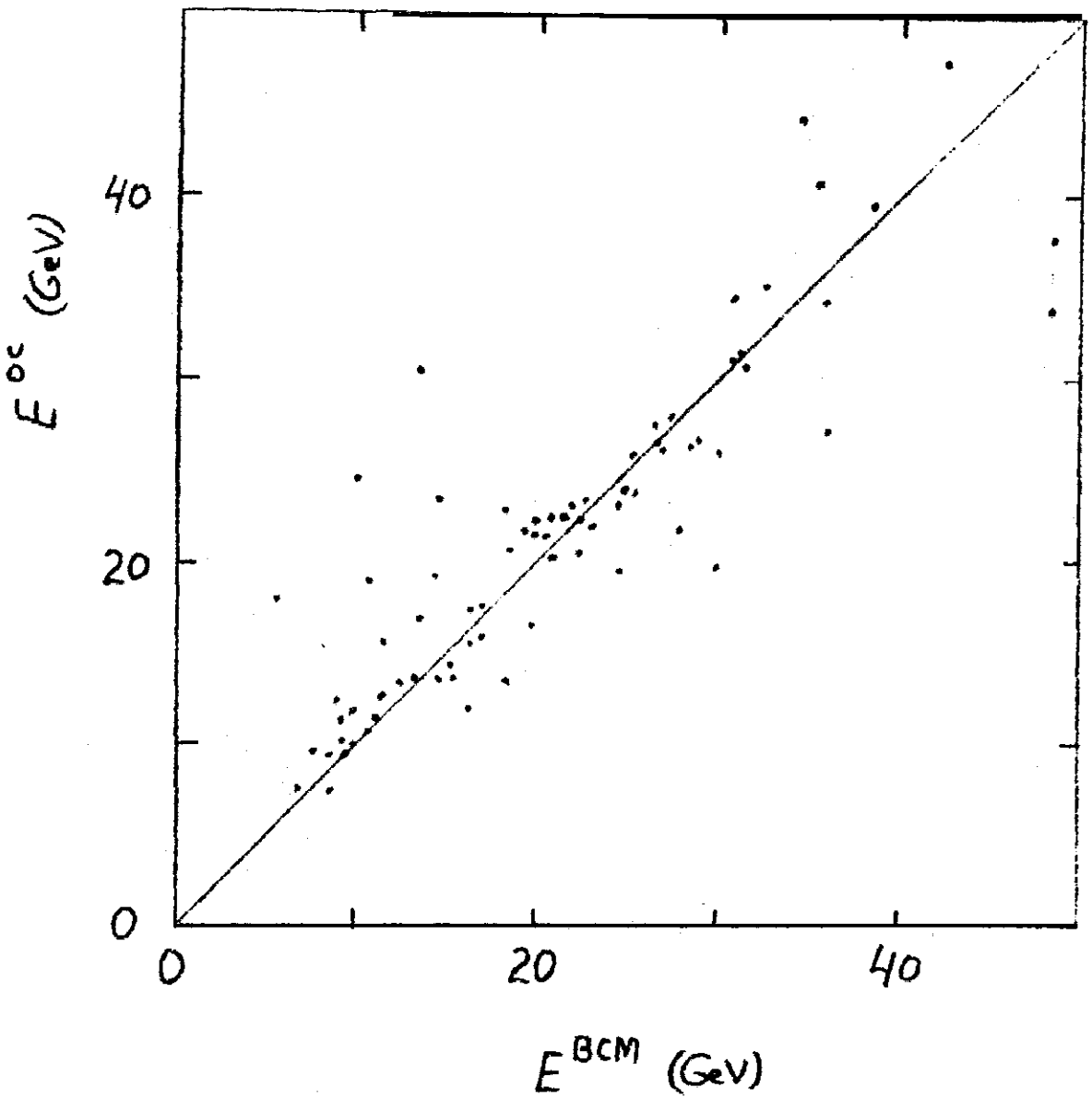

Fig 4a

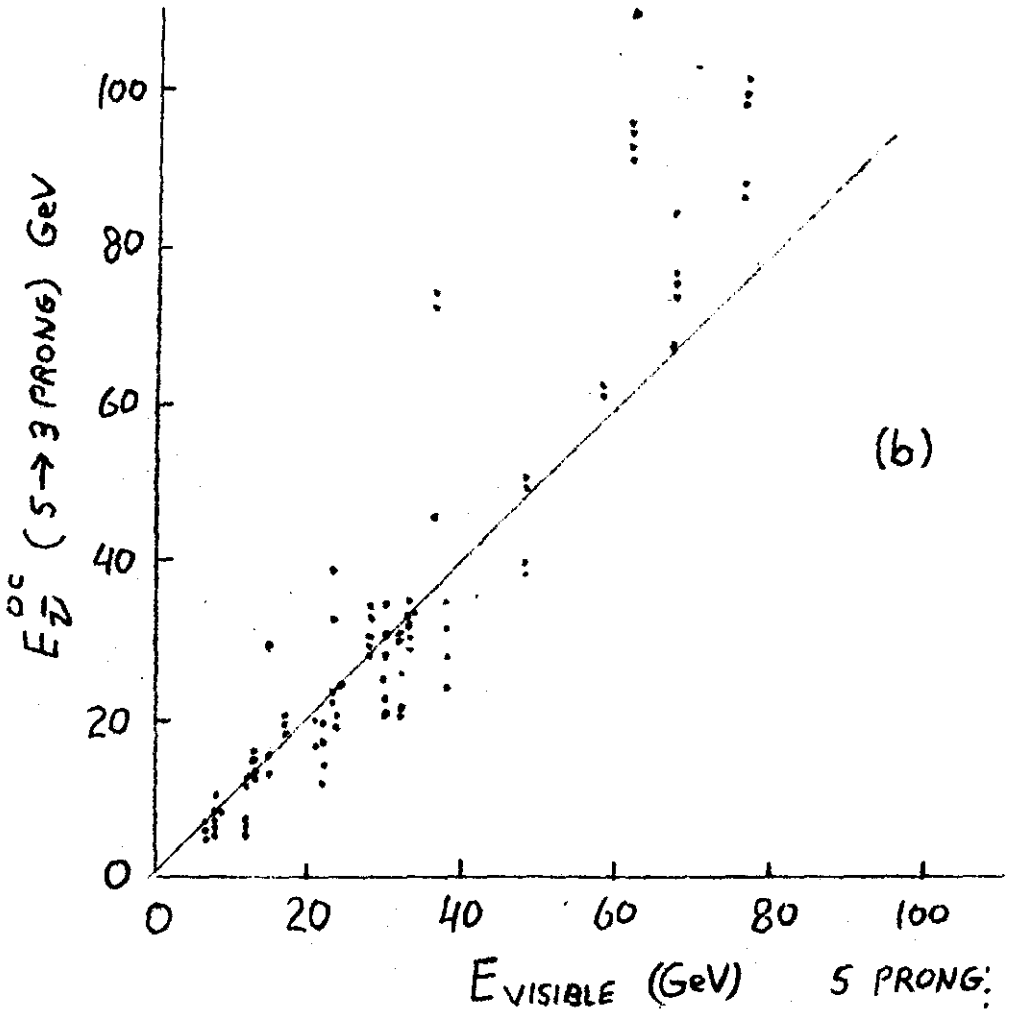
100
80
60
40
20
0
0
20
40
60
80
100
$E_{\bar{\nu}}^{oc}$ (5→3 PRONG) GeV
$E_{VISIBLE}$ (GeV)
(b)
5 PRONG

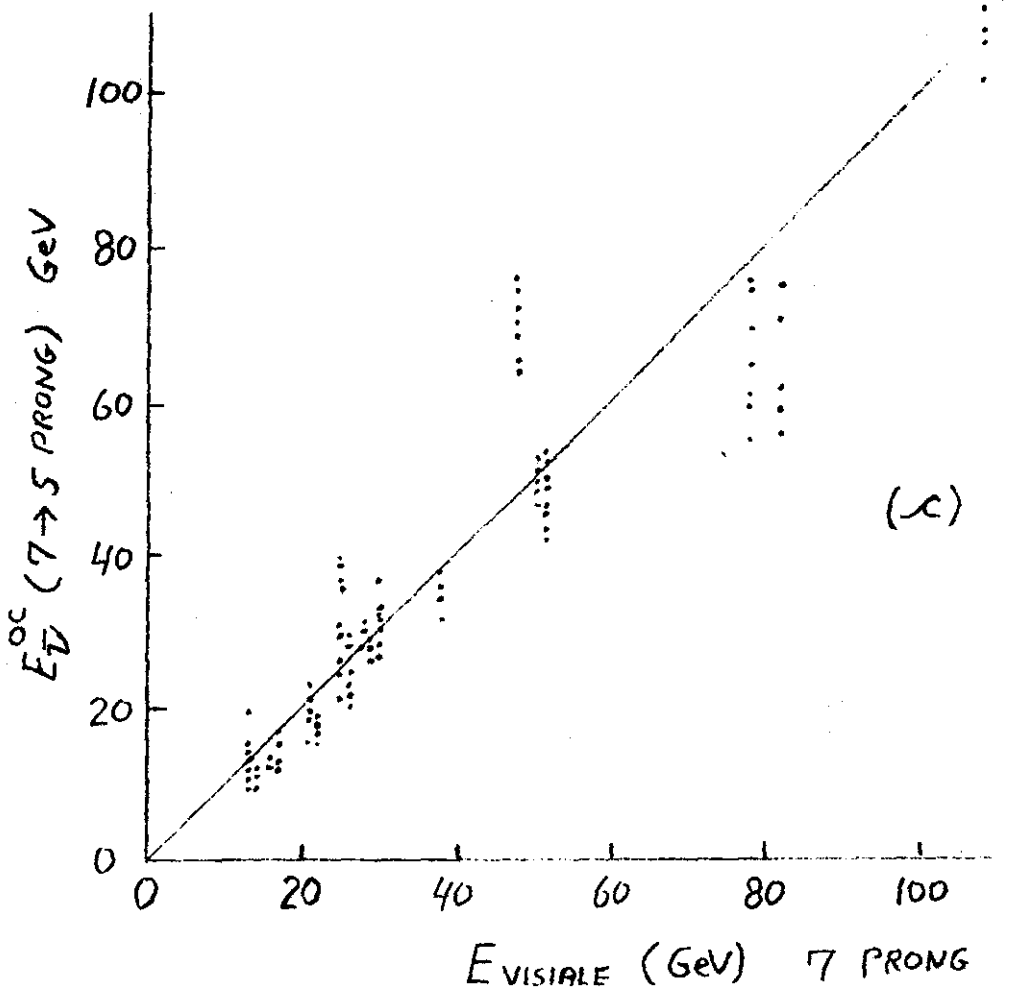
100
80
60
40
20
0
0
20
40
60
80
100
$E_{\bar{\nu}}^{oc}$ (7→5 PRONG) GeV
$E_{VISIBLE}$ (GeV)
(c)
7 PRONG

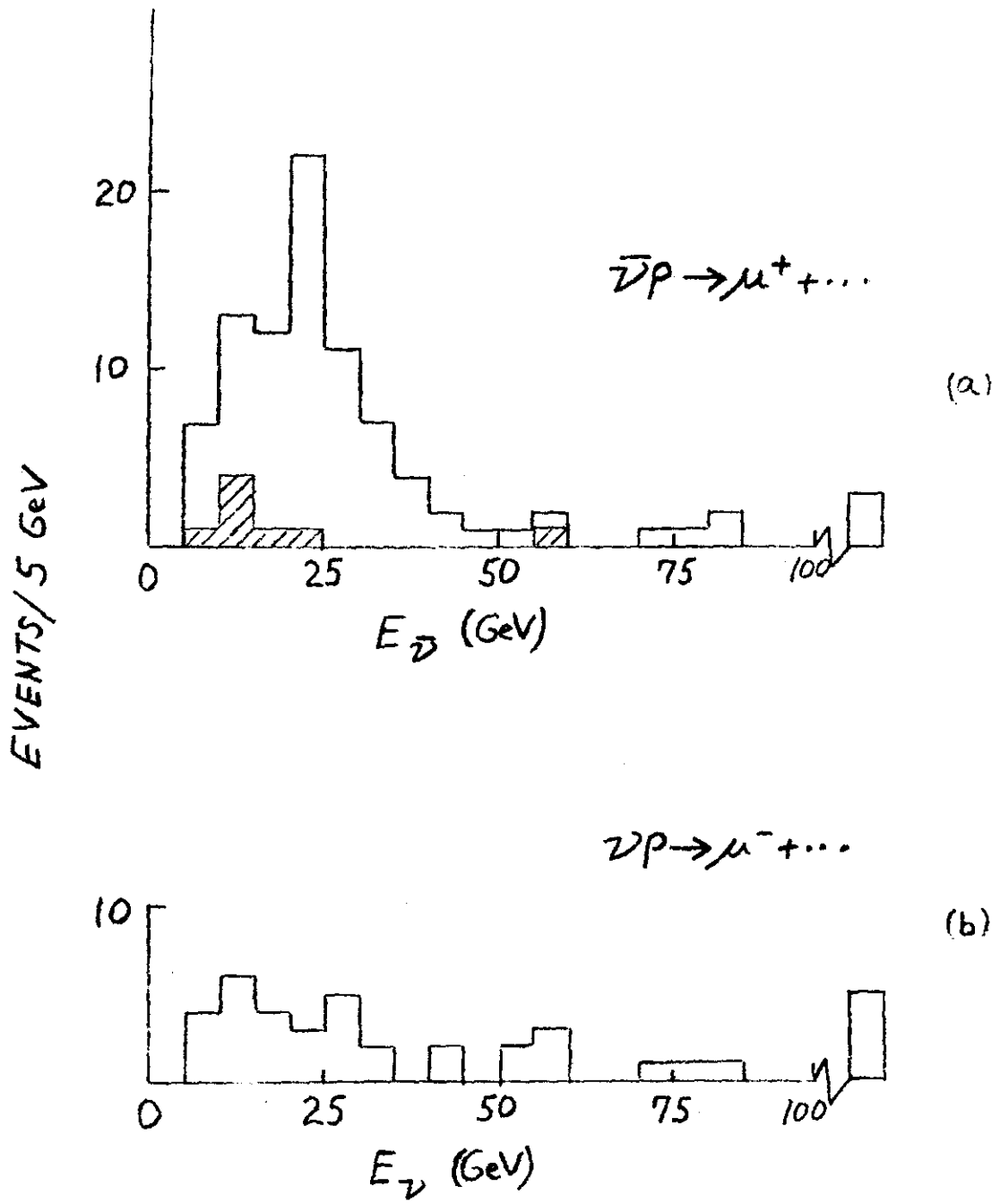
EVENTS/5 GeV
20
10
0
25
50
75
100
$\bar{\nu}p \to \mu^+ + \cdots$
$E_{\bar{\nu}}$ (GeV)
(a)
$\nu p \to \mu^- + \cdots$
10
0
25
50
75
100
E_ν (GeV)
(b)

Fig. 5

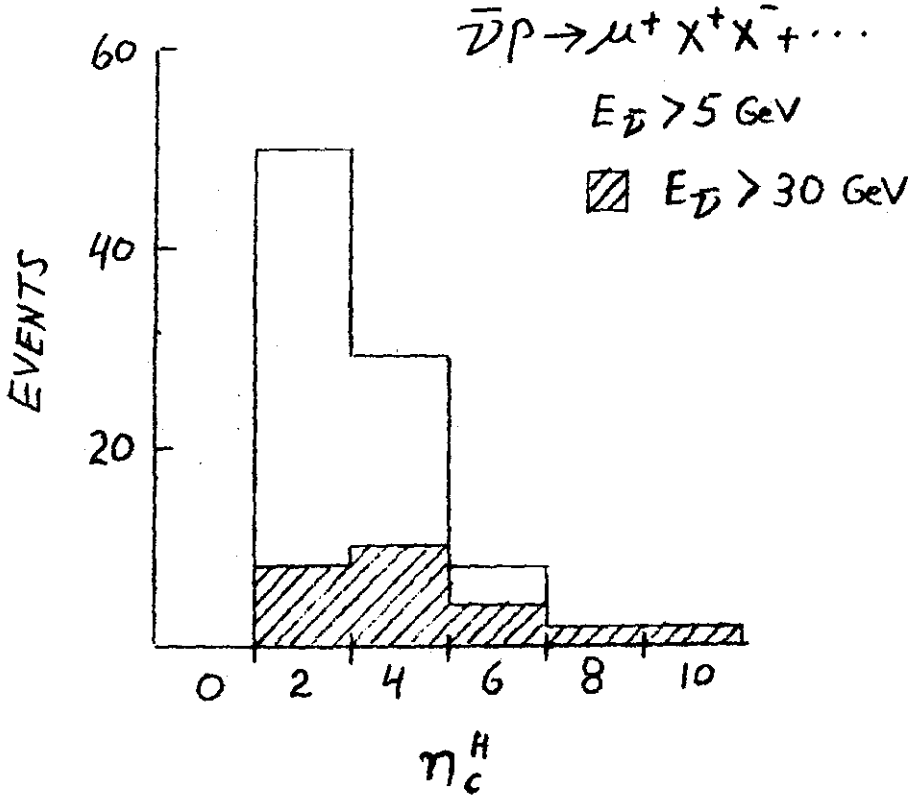
$\bar{\nu}p \to \mu^+ X^+ X^- + \cdots$
$E_{\bar{\nu}} > 5$ GeV
$E_{\bar{\nu}} > 30$ GeV
EVENTS
60
40
20
0
2
4
6
8
10
n_c^H

Fig. 6

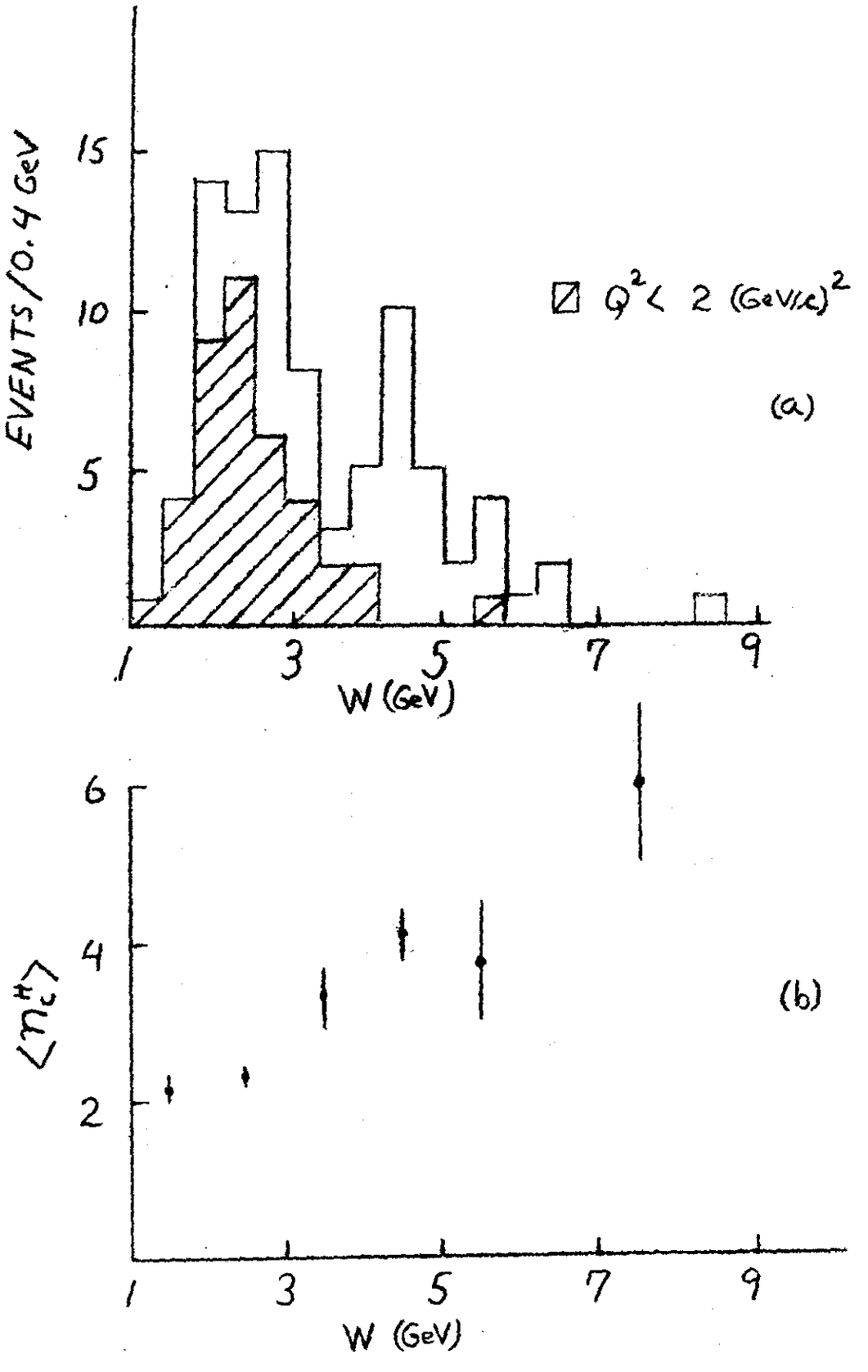
EVENTS/0.4 GeV
15
10
5
$Q^2 < 2$ (GeV/c)^2
(a)
1
3
5
7
9
W (GeV)
$\langle n_c^{\pm} \rangle$
6
4
2
(b)
1
3
5
7
9
W (GeV)

Fig. 7

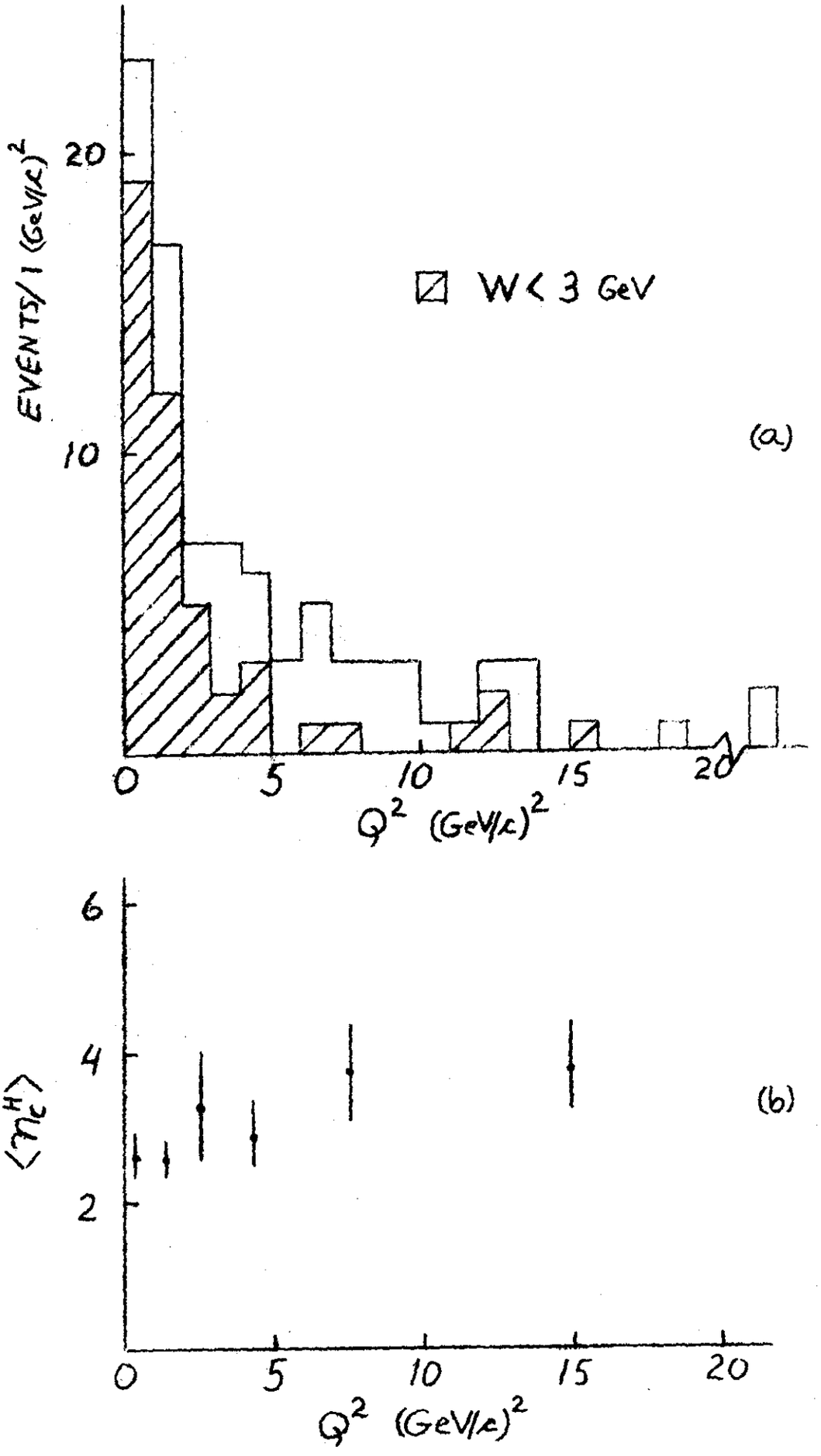
EVENTS/1 (GeV/c)^2
20
10
W < 3 GeV
(a)
0
5
10
15
20
Q^2 (GeV/c)^2
$\langle n_c^H \rangle$
6
4
2
(b)
0
5
10
15
20
Q^2 (GeV/c)^2

Fig. 8

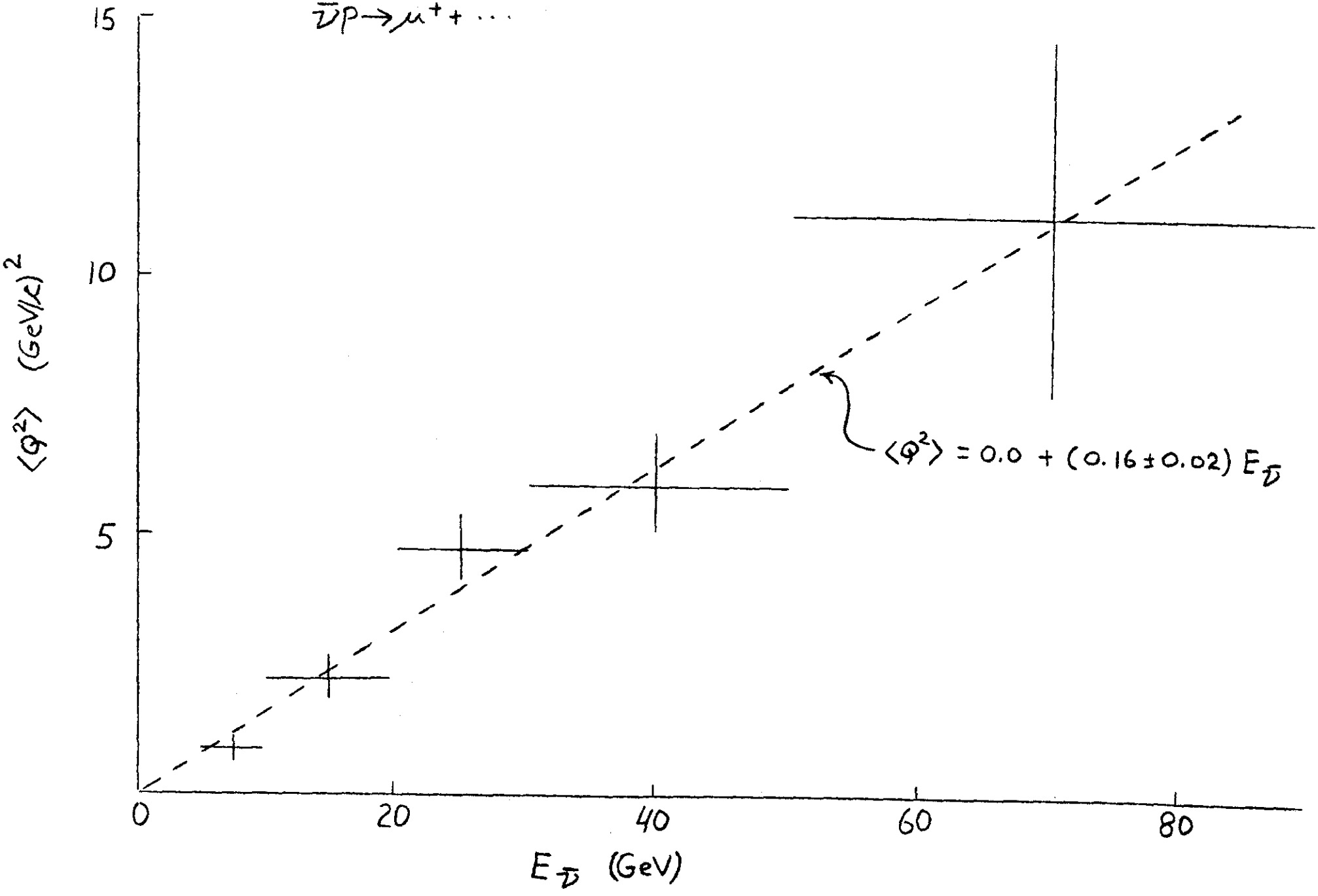
$\bar{\nu}p \to \mu^+ + \cdots$
15
10
5
0
20
40
60
80
$\langle Q^2 \rangle$ (GeV/c)^2
$E_{\bar{\nu}}$ (GeV)
$\langle Q^2 \rangle = 0.0 + (0.16 \pm 0.02)\, E_{\bar{\nu}}$

Fig. 9

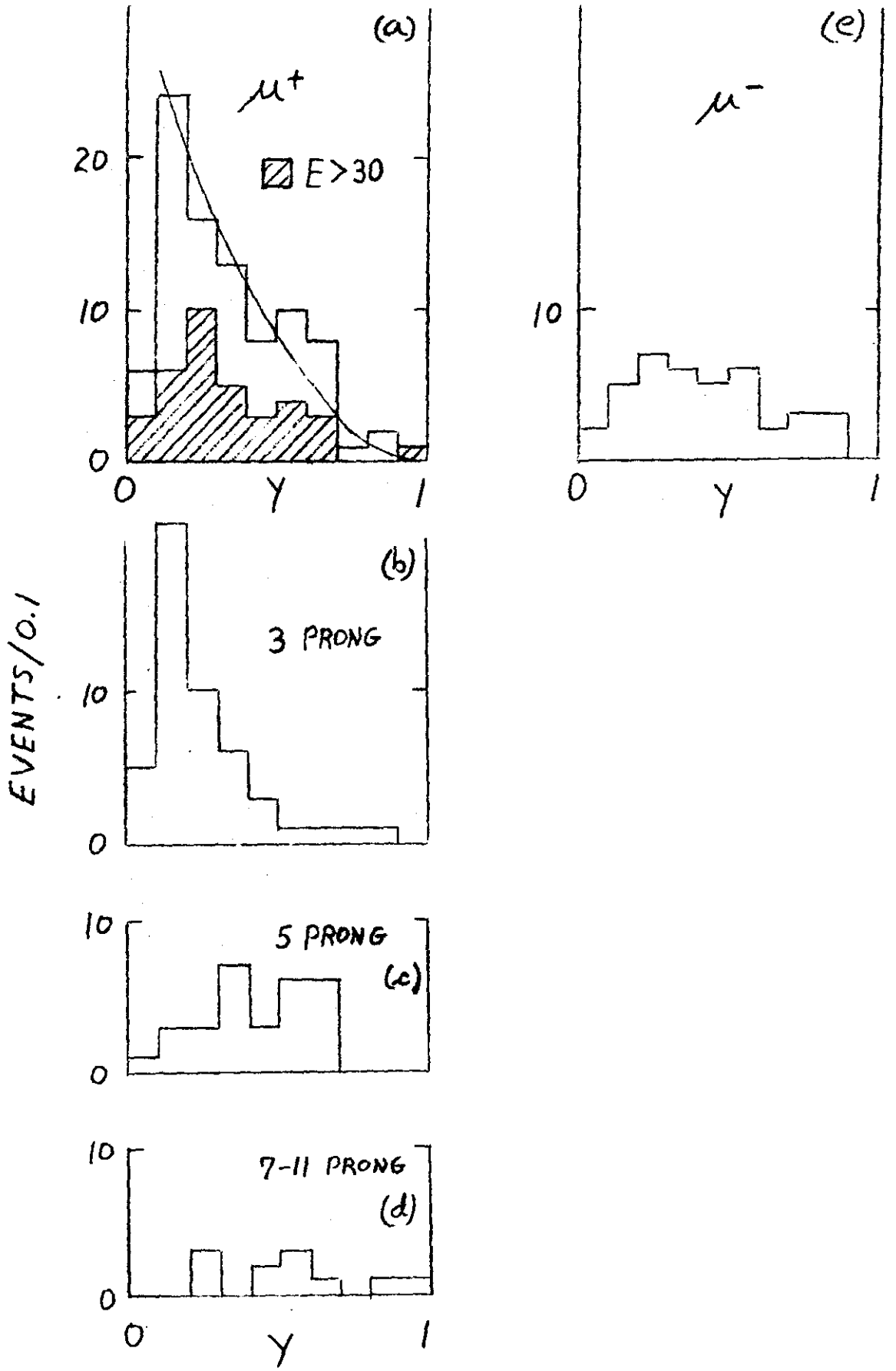
(a)
μ^+
E>30
20
10
0
0
Y
1
(e)
μ^-
10
0
Y
1
EVENTS/0.1
(b)
3 PRONG
10
0
10
5 PRONG
(c)
0
10
7-11 PRONG
(d)
0
0
Y
1

Fig. 10

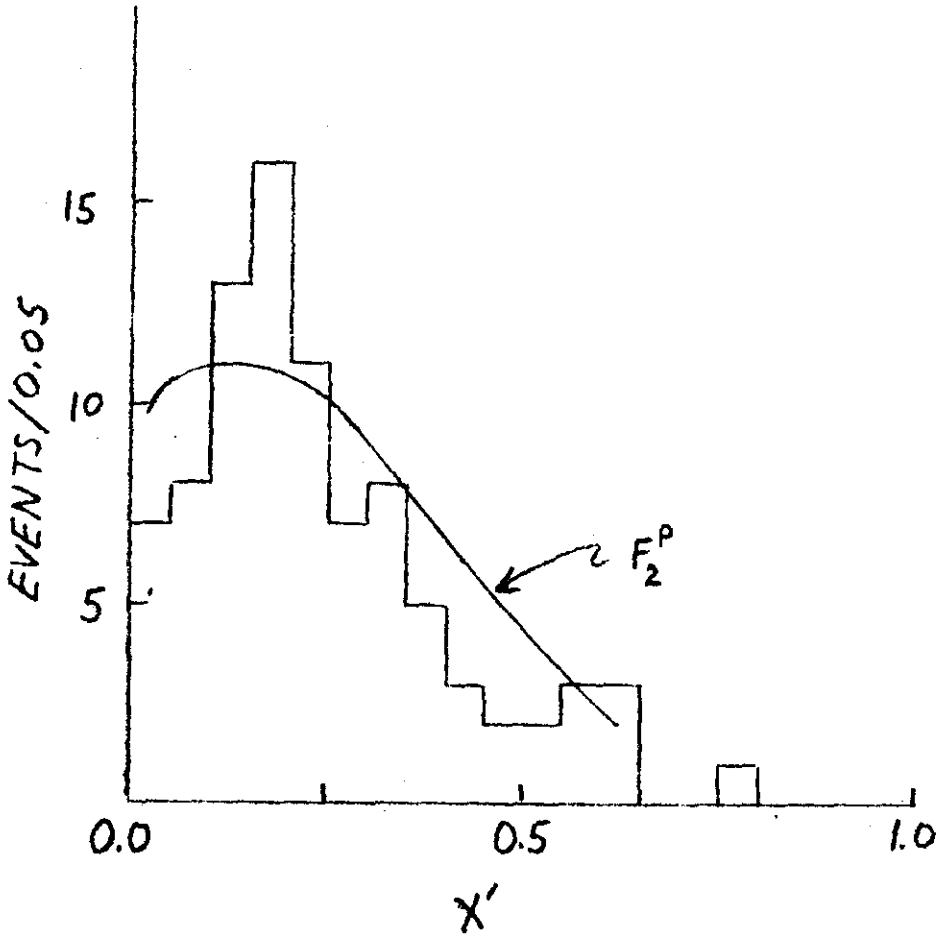

Fig. 11

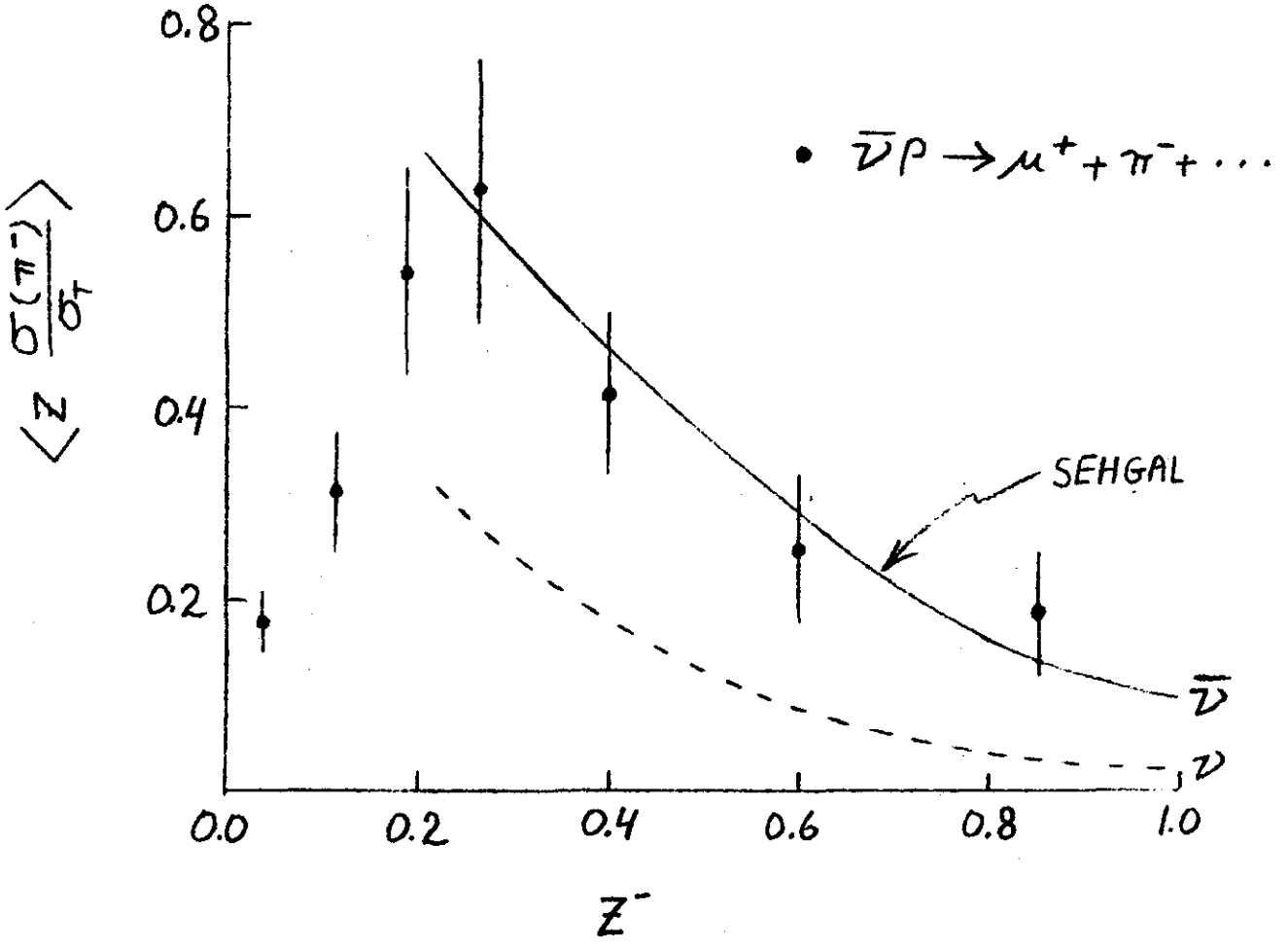
0.8
0.6
0.4
0.2
0.0
0.2
0.4
0.6
0.8
1.0
$\langle z \frac{\sigma(\pi^-)}{\sigma_T} \rangle$
z^-
$\bar{\nu} p \to \mu^+ + \pi^- + \cdots$
SEHGAL
$\bar{\nu}$
ν

Fig. 12